Sliding Mode Control for Hybrid Mass Dampers: Experimental analysis on robustness

Jonathan Rodriguez, Louis Mesny, Simon Chesné

Sliding Mode Control for Hybrid Mass Dampers : Experimental Analysis on Robustness

Jonathan Rodriguez, Louis Mesny and Simon Chesné

Univ Lyon, INSA Lyon, CNRS, LaMCoS, UMR5259, 69621 Villeurbanne, France. Author email: jonathan.rodriguez@insa-lyon.fr

Abstract

This manuscript presents an experimental investigation into the effectiveness of Sliding Mode Control (SMC) for vibration mitigation of a structure equipped with a Hybrid Mass Damper (HMD), as compared to conventional linear controllers. The experimental setup involves a cantilever beam exhibiting a first bending mode at 21Hz, subjected to strong parametric uncertainties and external excitation through a shaker. Additionally, an inertial actuator with internal resonance at 21Hz is utilized to apply passive and active control to the vibrating beam. The SMC approach is compared to three more common HMD control methods: $\alpha-$controller, LQG, and passivity-based control. To highlight the robustness and performance advantages of SMC, the nominal system undergoes significant mass and inertia modifications, not accounted for during the tuning of the observer and the controllers. The performances of the various controllers are then compared on four scenarios: two nominal identified systems and two configurations with uncertain parameters. Experimental results underscore the superior capabilities of SMC in mitigating structural vibrations, showcasing not only enhanced stability but also superior performance when confronted with substantial parametric uncertainties, outperforming traditional linear control methods.

Keywords: Sliding mode control, Nonlinear control, Tuned mass damper, Hybrid mass damper, Robust control, Uncertain system

1. Introduction

The Tuned Mass Damper (TMD) is one of the most widely used passive anti-vibration device [1, 2] in many application fields, especially in civil engineering for seismic concerns or transportation since vibrations are inherent to any vehicle dynamics. They usually consist of a suspended mass, a spring, and a dash-pot attached to the primary structure disturbed by an external source of vibration. TMDs must be tuned properly in mass and stiffness such that

⋆Fully documented templates are available in the elsarticle package on CTAN.

their eigenfrequency matches the targeted mode on the primary structure or bandwidth. Damping tuning must also be addressed [3, 4] in order to display optimal passive control performances.

However, one of the major flaws of passive TMDs is their high sensitivity to the primary system eigenstructure. Yet, the modal response of transportation systems can vary drastically with excitation amplitude due to structural nonlinearities [5] or with time due to configuration changes in mass distribution or payload variations. The external excitation can also shift in the frequency domain as is the case for rotating machines with a variable angular velocity typically or seismic excitation [6, 7]. Hence, many methods have been developed in the last decades to improve TMDs vibration control performances and robustness to parametric changes in the primary structure.

Although not within the scope of this manuscript, it should be mentioned as one the directions possible to improve the TMDs efficiency non-linear passive solutions also called Non-linear Energy Sinks (NES) [8, 9]. These passive vibration mitigation systems exhibit time-varying eigenfrequencies in response to the excitation amplitude of the host structure, enabling a broader frequency range for energy transfer between the primary structure and the proof mass. However, the implementation of such passive systems necessitates precise tuning of their mechanical properties to ensure optimal performance.

An other efficient method to improve the performances of TMDs is active control also called hybridization since the actuator is added in parallel with the tuned spring and dash-pot forming a Hybrid Mass Damper (HMD). Among the numerous linear controllers applied to HMDs, one can find classical control methods such as PID control, Optimal control, H-infinity optimization [10, 11] or more physically oriented controllers like Direct Velocity Feedback (DVF), Integral Force Feedback (IFF) or acceleration feedback [12], α-controller [13], Dual-loop control [14] or Skyhook inspired control [15, 16]. Such control methods can easily enhance the TMD passive behavior by increasing the vibration attenuation and also enlarging the isolation bandwidth. Nevertheless, the performance limits of active control are generally imposed by stability concerns. Besides, stability margins quickly reduce or even disappear when the primary structure suffers significant variations in its modal response due to the reasons mentioned earlier. As a consequence, the control can possibly degrade the vibration level on the structure achieved with passive control by spill-over effect or even be unstable.

To tackle the weaknesses of linear control when facing significant parametric uncertainties in uncertain systems, nonlinear robust control methods have been developed for robotics applications first and seismic isolation as Sliding Mode Control (SMC). A sliding surface is defined as a manifold expressed by linear or nonlinear operators of the system states, modal or physical. Then, the dynamics of the closed-loop system are reduced to those of the sliding variable and forced to reach the sliding surface with a switching control signal depending on the sign of the sliding variable $i.e$ the system position in the phase space with respect to the sliding manifold. Different methods have been developed to compute the desired sliding surface like Optimal SMC (OSMC) [17] based on linear quadratic

minimization. Frequency-shaped sliding surfaces have also been proposed first by Young and Ozguner [18] and developed further by Zuo and Slotine [19] for vibration mitigation.

Adhikari et al. [20] applied SMC to the control of HMDs on top of buildings for seismic vibrations only considering the state of the upper floor and highlighted the robustness of the method. Later, new developments and applications in vibration control using SMC have shown its performance interest when applied to smart structures [21], nonlinear Duffing systems [22] or systems with time delays [23].

Concha et al. [24] proposed recently a tuning method for HMD control using SMC based on Ackermann's formula and the original work of Ackermann and Utkin [25]. The authors compared the performances with the classical linear LQR approach and also OSMC taking into account explicitly the constraint of control signal amplitude. However, the robustness to uncertainties was not specially addressed with the experimental setup. Adaptive SMC has also been proposed to provide additional robustness capabilities to SMC. In [26], an adaptive fuzzy SMC has been applied to vibration control of a beam with parametric uncertainties due to mass addition leading to a 19% variation of the first modal frequency. More recently, Hu et al. [27] used an adaptive disturbance observer to handle the uncertainties in wind turbines and reduce the dynamic loads. Nevertheless, if robustness is one of the main features of all the existing SMC-derived methods, it is not always illustrated experimentally in vibration control applications, especially in higher frequencies than seismic excitation.

The contribution of the following paper is to experimentally emphasize the robustness advantages of SMC in addressing vibration mitigation problems with substantial parametric uncertainties when applied to HMDs. Thus, such nonlinear control method is rarely used for vibration control at higher frequencies than seismic excitation or in the context of TMD hybridization. The second part of the contribution is that few studies address practical robustness problems due to strong parametric uncertainties in the aforementioned vibration control context using SMC. Here, this nonlinear control method is compared against three other controllers on a cantilever beam with additional/removable mass to shift its modal response to lower or higher frequencies. These controllers are representative of diverse common approaches in control theory. Furthermore, the observer design exclusively focuses on the first bending mode of the beam to showcase the performance of the different controllers in handling unmodeled dynamics. By doing so, the study effectively highlights the efficacy of SMC in managing uncertainties and its potential superiority over alternative control methods for HMDs.

The manuscript is organized as follows: the section 2 introduces the experimental setup with its different nominal and uncertain configurations, and respective identifications. Section 3 then develops the four different controllers, including SMC to be tested on the control of the HMD. Finally, section 4 presents and summarizes all the experimental results obtained and compares the SMC performance and robustness to the three other controllers.

2. System definition and identification

In this section, the experimental setup is presented with the identification method and associated results.

2.1. Experimental setup

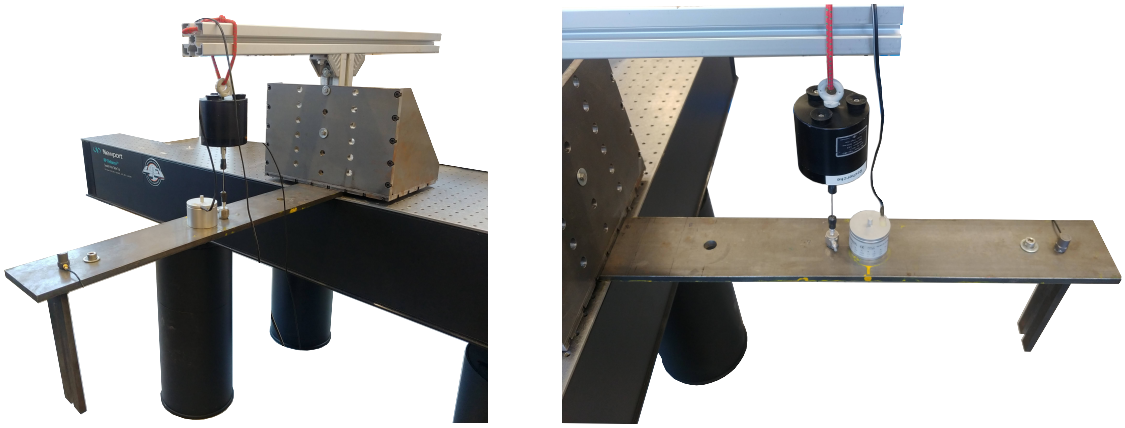

(a) (b)

Figure 1: Experimental setup, nominal system B with additional mass.

The experimental system considered in this manuscript is a steel clamped beam of dimensions 600×100×10mm as displayed in Figure 1 and in the corresponding scheme in Figure 2. An electrodynamic shaker applies a vertical disturbance force to the structure and a sensor measures the acceleration close to the free end of the beam. Besides, a Micromega inertial actuator is also placed approximately in the middle of the cantilever, close to the perturbation force application point. This actuator, whose principle is detailed in Figure 3 acts first as an optimized passive TMD device (Tuned Mass Damper) with a moving mass of 160g, an internal resonance tuned at 21Hz and approximately 11% of damping factor. In addition to stiffness k and viscous damping c, the inertial actuator is also constituted of a coil with a permanent magnet allowing control of the force between the beam and the reaction mass with a current signal input $i_{control}$.

In order to test the robustness capabilities of the different controllers, two nominal systems, both with the first bending mode at 21Hz are to be identified:

- Nominal system A : clamped beam of dimensions 616×100×10mm,
- Nominal system B : clamped beam of dimensions 536×100×10mm with additional mass of 0.9kg.

Then, two uncertain configurations are to be tested:

- Uncertain system A : nominal system A with additional mass of 0.9kg.

- Uncertain system B : nominal system B without the additional mass of 0.9kg.

The additional mass used in this context to add parametric uncertainties in the closed-loop provides a substantial mass variation $i.e$ between 18.6 and 21.4%. The objective here is to shift significantly the system modal frequencies to highlight the different controllers robustness characteristics.

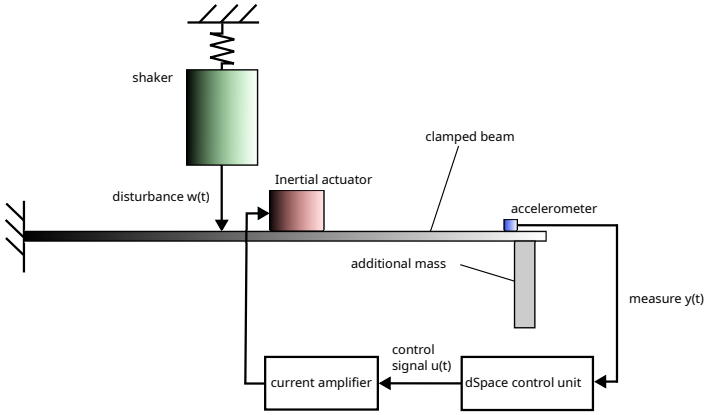

Figure 2: Scheme of the experimental setup, nominal system B with additional mass.

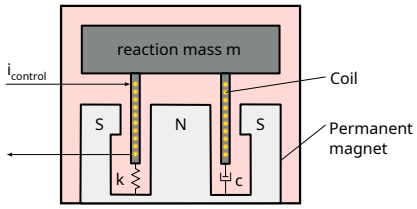

Figure 3: Scheme of the inertial control actuator.

2.2. Identification of the system

Let us now define $H_0(s)$ the transfer function between the electrodynamic shaker input disturbance $w(t)$ and the accelerometer output signal $y(t)$, and $H_1(s)$ the transfer function between the inertial actuator input $u(t)$ and the accelerometer signal $y(t)$ with s as the Laplace variable. Since the objective of the control is to assist and enhance the performances of the passive TMD, only the first mode of the beam will be considered in the model of $H_1(s)$. It is also well known that the addition of the TMD device on the beam adds another mode to the original system [2].

Accordingly, the Figure 4 displays the considered simplified model of the structure with 2 degrees of freedom where m_0 is the modal mass of the cantilever 1^{st} bending mode added to the TMD fixed mass, m_1 is the TMD mobile mass,

k_0 is the modal stiffness of the 1^{st} bending mode, k_1 the stiffness of the TMD, x_0 and x_1 are the spatial coordinates of the masses and F is the force control input.

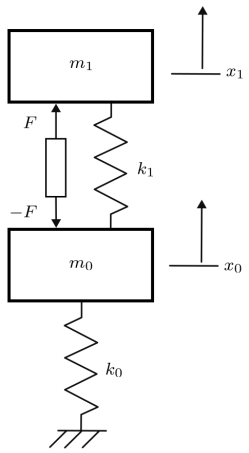

Figure 4: Dynamic system model.

For the sake of simplicity, the damping is not considered when deriving the system equations of motion given by:

$$m_0\ddot{x}_0 = -F - k_1(x_0 - x_1) - k_0 x_0 \quad (1)$$
$$m_1\ddot{x}_1 = F + k_1(x_0 - x_1) \quad (2)$$

In the Laplace domain, the transfer function between the acceleration of the beam $\ddot{x}_0$ and the control input F is then written from (1) as:

$$\frac{\ddot{X}_0}{F}(s) = \frac{-m_1 s^4}{(m_0 s^2 + k_0 + k_1)(m_1 s^2 + k_1) - k_1^2} \quad (3)$$

According to the previous equation, we know model $H_1(s)$ as a 4^{th} order proper transfer function with 2 pairs of conjugate poles and 2 pairs of zeros. The zeros are not defined as pure derivators to keep some design freedom and be able to correct the phase of H_i afterwards within the control bandwidth.

Thereby, $H_1(s)$ can be written as a product of two proper transfer function of order 2:

$$H_1(s) = \prod_{i=1}^{2} \frac{(s - z_{i,1})(s - z_{i,2})}{s^2 + 2\xi_i\omega_i s + \omega_i^2} \quad (4)$$
$$= \prod_{i=1}^{2} H_{1,i}(s) \quad (5)$$

with $(z_{i,1}, z_{i,2}) \in \mathbb{C}^2$, $\omega_i \in \mathbb{R}^+$ is the frequency of the i^{th} pole pair in $rad.s^{-1}$ and $\xi_i \in \mathbb{R}^{+*}$ the damping ratio. We now define a state space realization for each intermediate sub-function $H_{1,i}(s)$ as:

$$H_{1,i} \begin{cases} \dot{x_i} = A_i x_i + B_i u_i \\ y_i = C_i x_i + D_i u_i \end{cases} \tag{6}$$

with $x_i \in \mathbb{R}^2$ the state vector, $u_i \in \mathbb{R}$ and $y_i \in \mathbb{R}$ respectively the input and output of system $H_{1,i}$. One possible realization of the state space system (A_i, B_i, C_i, D_i) is:

$$A_i = \begin{bmatrix} 0 & 1 \\ -\omega_i^2 & -2\xi_i\omega_i \end{bmatrix}, B_i = \begin{bmatrix} 0 \\ 1 \end{bmatrix}, D_i = 1 \tag{7}$$

where the unitary gain in the control matrix B_i is a design choice. Let us now define two possible cases for the system zeros z_i. In the first case, the identified zeros are both real such that $z_{i,1} = a_1$ and $z_{i,2} = a_2$ with $(a_1, a_2) \in \mathbb{R}^2$. Then C_i can be defined as:

$$C_i = \begin{bmatrix} a_1 a_2 - \omega_i^2, & -(a_1 + a_2) - 2\xi_i\omega_i \end{bmatrix} \tag{8}$$

If the identified zeros are a pair of conjugate complex such that $z_{i,1} = a_1 + ib_1$ and $z_{i,1} = a_1 - ib_1$ with $(a_1, b_1) \in \mathbb{R}^2$. Then C_i can be defined as:

$$C_i = \begin{bmatrix} a_1^2 + b_1^2 - \omega_i^2, & -2a_1 - 2\xi_i\omega_i \end{bmatrix} \tag{9}$$

Thus, the total transfer function $H_1(s) = H_{1,1}(s)H_{1,2}(s)$ can be defined by the following state space realization:

$$H_{1,i} \begin{cases} \dot{x'} &= A'x' + B'u \\ y &= C'x' + D'u \end{cases} \tag{10}$$

with $x' \in \mathbb{R}^4$ the state vector such that $x' = [x_1^T \ x_2^T]^T$, $u \in \mathbb{R}$ the voltage control input and $y \in \mathbb{R}$ the voltage output of the accelerometer. The matrices $A' \in \mathbb{R}^{4\times4}$, $B' \in \mathbb{R}^{4\times1}$, $C' \in \mathbb{R}^{1\times4}$ and $D' \in \mathbb{R}$ are defined as:

$$\begin{aligned} A' &= \begin{bmatrix} A_1 & \mathbf{0}_{2\times2} \\ B_2C_1 & A_2 \end{bmatrix}, B' = \begin{bmatrix} B_1 \\ B_2D_1 \end{bmatrix} \\ C' &= \begin{bmatrix} D_1C_1 & C_2 \end{bmatrix}, D' = D_2D_1 \end{aligned} \tag{11}$$

Considering that this realization is not well balanced in terms of controllability and observability, the Gramian method [28] is applied to the system (A', B', C', D') by a coordinate transformation defining a new state vector $x = T^{-1}x'$ with $T \in \mathbb{R}^{4\times4}$. The new realization of H_1 is now defined by:

$$H_1 \begin{cases} \dot{x} = Ax + Bu \\ y = Cx + Du \end{cases} \tag{12}$$

with $A = T^{-1}A'T$, $B = T^{-1}B'$, $C = C'T$, and $D = T^{-1}B'$.

To identify $H_1(s)$, a white noise of RMS value 1.6V and sampling frequency 10kHz is applied to the current amplifier connected to the HMD. The measured and identified transfer functions $H_1(f)$ are displayed in Figure 5 for the nominal systems A and B. The identified poles and zeros are summarized in Table 1. As desired, the poles of the nominal systems corresponding to the first two modes are very close to each other. As for the zeros, their placement has been tuned to obtain the best curve-fitting within the control bandwith corresponding to the vicinity of the 1^{st} bending mode. As mentioned earlier, they were not defined as pure derivators to allow phase correction close to the controlled eigenfrequencies. Such angular correction could be due to non-perfect experimental boundary conditions from the beam clamping and its support table whose low frequency dynamics are close enough to the beam first mode to disturb the system.

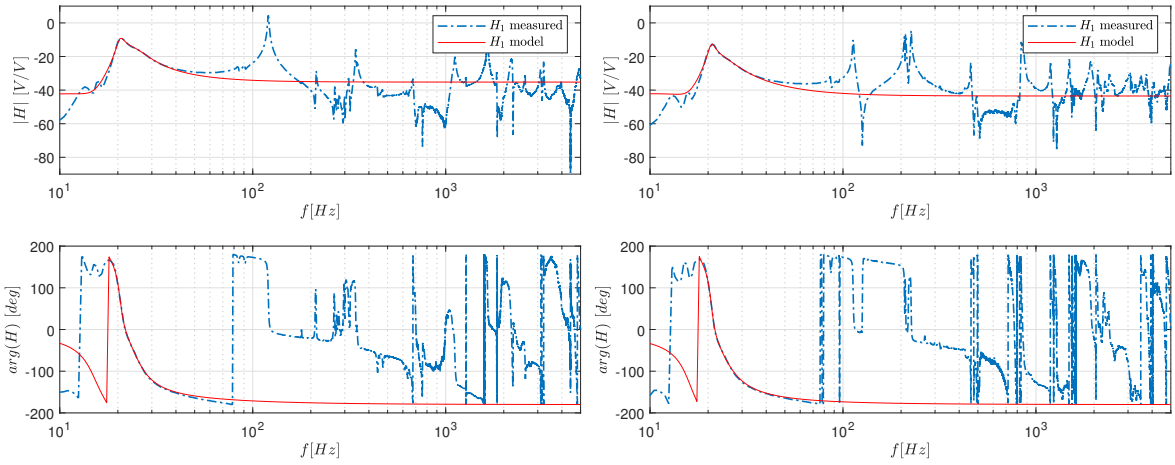

Figure 5: Measured and identified transfer functions $H_1(f)$ for (a) nominal system A, and (b) nominal system B.

-	-	A	B
$H_{1,1}$	poles	$-5.53 + 129i$ $-5.53 - 129i$	$-5 + 130.6i$ $-5 - 130.6i$
	zeros	$14.6 + 94.1i$ $14.6 - 94.1i$	$13.9 + 99.6i$ $13.9 - 99.6i$
$H_{1,2}$	poles	$-27.3 + 152.4i$ $-27.3 - 152.4i$	$-32.5 + 148.6i$ $-32.5 - 148.6i$
	zeros	-132.9 130	-228 188

Table 1: Identification parameters.

Finally, Figure 7 displays the measured nominal and uncertain systems de-

fined earlier through $H_1(f)$. Mainly, the first bending mode of the beam is shifted in frequency from 21Hz (nominal A and B) to 17.5Hz or 26Hz giving an interesting variation of +24%/-17% in modal frequency for the robustness estimation of the different controllers.

To complete the analysis of the nominal systems, the transfer functions H_0 defining the frequency response function between the exogenous perturbation from the shaker and the error sensor *i.e* the accelerometer, are measured by applying also a white noise of RMS value 2.21V and sampling frequency 10kHz to the shaker amplifier. The results for systems A and B are displayed in Figure 6. It is worth noticing that even if nominal systems A and B are set to have the first beam bending mode at 21Hz, they present different mass ratios and inertia distribution which obviously impacts the global effect of the HMD on the beam vibration and the overall frequency response of the system.

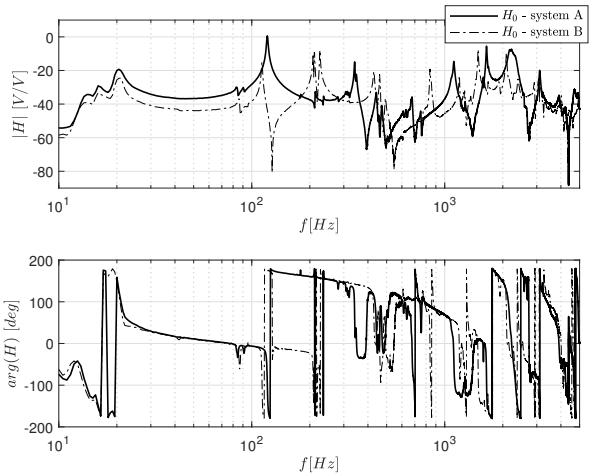

Figure 6: Measured transfer functions $H_0(f)$ for nominal systems A and B.

3. Control design

In the following section, 3 different controllers, representative of different common approaches in control theory, are introduced to control the identified nominal system (12) in addition with SMC: α-controller, LQG and passivity-based control. The αcontroller uses a velocity feedback method with no need of observer, LQG is one of the most widely used optimal control method but comes with the additional constraint of the need for a properly designed observer. Finally, passivity-based control is in general used for systems with non-negligible parametric uncertainties due its inherent robustness.

3.1. α-controller

This controller introduced by Colette et al. [13] is specially designed for the control of HMD since it only requires as input the velocity of the primary

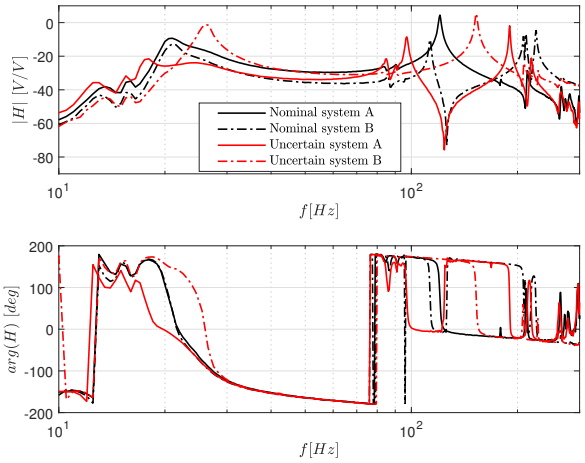

Figure 7: Measured transfer functions $H_1(f)$ for nominal and uncertain systems A and B.

structure at the application point of the active device. Defining $v \in \mathbb{R}$ as the measured velocity of the beam, the control signal u is theoretically:

$$u = -k_\alpha \frac{(s+\alpha)^2}{s^2} v \tag{13}$$

$$= -K_\alpha(s) v \tag{14}$$

with $k_\alpha \in \mathbb{R}^+$ the control gain and $\alpha \in \mathbb{R}$ the main tuning parameter of the controller where the optimal theoretical tuning is $\omega_1 < \alpha < \omega_2$.

However, the denominator of $K_\alpha(s)$ adds 2 marginally stable poles in the open loop transfer function. Thus, the controller must be modified to avoid any offset in the command signal since the measured acceleration must also be integrated first before applying the control law. Hence, a high pass integrator F in the form $1/(s+\omega_{int})$ with $\omega_{int} \in \mathbb{R}^+$ and $\omega_{int} << \omega_i \; \forall i \in [1,2]$ is added to the feedback loop between the measurement y from the accelerometer and the α-controller. Similarly, the marginally stable poles of $K_\alpha(s)$ are slightly shifted to guarantee the stability of the open loop such that:

$$K_\alpha = -k_\alpha \frac{(s+\alpha)^2}{(s+\omega_{int})^2} \tag{15}$$

Finally, the Figure 8 displays the block diagram of the control loop. The transfer function $H_{cl}(s)$ between the perturbation w and the measurement y is defined by:

$$H_{cl}(s) = H_0(s) \left(I + H_1(s) K_\alpha(s) F(s)\right)^{-1} \tag{16}$$

where the objective of the control is to minimize $||H_{cl}(s)||_\infty$ by choosing properly α and k_α.

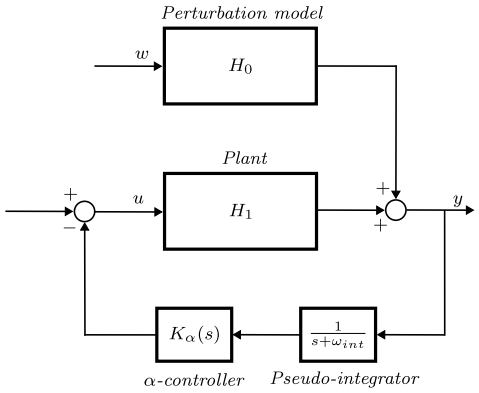

Figure 8: α-controller diagram.

3.2. LQG

The next linear controller being compared to robust nonlinear control is LQG, or the widely used linear quadratic regulator in addition with a Kalman observer. Let us define the control gain matrix $K \in \mathbb{R}^{1\times 4}$ such that the control signal $u = -Kx$ with x the state vector of system (12). Hence, K is determined by minimizing the following functional J:

$$J = \int_{t=0}^{\infty} x^T Q x + u^T R u \; dt \tag{17}$$

where $Q \in \mathbb{R}^{4\times 4}$ is positive definite and $R \in \mathbb{R}^{+*}$. Both matrices determine the control gain and so the stability margin with the linear quadratic regulator K.

Since the full state vector x is not available to feed the controller, a Kalman observer is designed to compute the estimation $\hat{x}$ of x. The observer is in the form of the following state space realization:

$$\dot{\hat{x}} = A\hat{x} + Bu + L\left(y - C\hat{x}\right) \tag{18}$$

where $L \in \mathbb{R}^{4\times 1}$ is the observer gain matrix. Thus, the control signal is defined by $u = -K\hat{x}$. The Figure 9 displays the block diagram of the LQG control loop.

3.3. Passivity-based control

The next controller to be applied uses the concept of passivity. The system is forced to reach a manifold $\sigma = Ex = 0$ and $\dot{\sigma} = 0$ with $\sigma \in \mathbb{R}$ and $E \in \mathbb{R}^{1\times 4}$. A simple nonlinear switching control feedback can be defined as:

$$u = -k_p sgn(\sigma) \tag{19}$$

with $k_p \in \mathbb{R}^+$. To guarantee the closed-loop stability, the linear operator E is determined with the principle of passivity using the Kalman-Yakubovitch-Popov lemma.

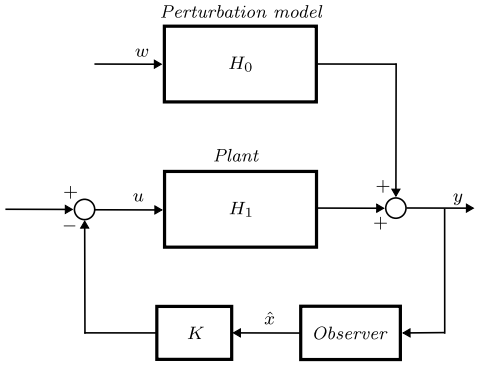

Figure 9: LQG controller diagram.

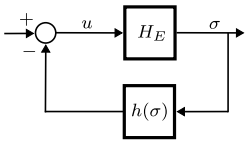

Figure 10: Lure's problem scheme with static nonlinear feedback.

First, the closed loop system is put into the form of Lure's problem where the static nonlinear part $h(\sigma) = k_p sgn(\sigma)$ is a feedback of the linear system H_E as displayed in Figure 10. The system H_E is written as:

$$H_E \begin{cases} \dot{x} &= Ax &+Bu \\ \sigma &= Ex \end{cases} \tag{20}$$

Since $h(\sigma)$ lies in the first and third quadrant, the passivity of the closed-loop is guaranteed if H_E is a positive real transfer function [29]:

Lemma 1. *Let $H_E(s) = E(sI - A)^{-1}B$ be a $m \times m$ transfer function matrix, where (A,B) is controllable and (A,E) is observable. Then $H_E(s)$ is strictly positive real if and only if there exist matrices $P = P^T > 0$ and G such that:*

$$PA + A^T = -G^T G \tag{21}$$

$$PB = E^T \tag{22}$$

For the sake of simplicity, we define $G = I$ and obtain P from the Lyapunov equation (21). Finally, the matrix E guaranteeing the close-loop stability for any gain $k_p > 0$ is given by $E = B^T P$. The block diagram of the passivity-based controller is shown in Figure 11 where the theoretical sign function is replaced by $\sigma/(|\sigma| + \epsilon)$ with $\epsilon \in \mathbb{R}^{+*}$, and $\epsilon << 1$ for practical implementation concerns due to chattering. Since the full state is not available, σ is defined by $\sigma = E\hat{x}$ with $\hat{x}$ the state estimation from Kalman observer (18).

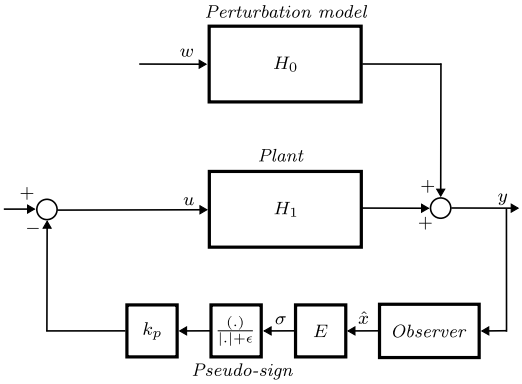

Figure 11: Passivity-based control diagram.

3.4. Sliding mode control

The last controller to be defined and applied to the experimental setup is based on the sliding mode control method [30]. The principle of such a method is to define first a sliding variable σ as a function, linear or nonlinear of the error. A reduced-order system is then defined depending only on the dynamics of the sliding variable. Finally, a switching control signal is applied to force the states of the reduced-order system to converge to the sliding surface defined *i.e* $\sigma = \dot{\sigma} = 0$.

The objective is to design a controller that constrains the trajectory of the system (12) to the manifold $\sigma = Sx = 0$ with $S \in \mathbb{R}^{1\times 4}$. The switching function S is to be defined later to guarantee closed-loop convergence. As shown in the corresponding block diagram in Figure 12, the control signal u is the addition of a linear equivalent control and a nonlinear switching control where the first part is not necessary to maintain the closed-loop stability.

Assuming the system is already on the sliding manifold such that $\sigma = \dot{\sigma} = 0$, from (12) we have:

$$S\dot{x} = SAx + SBu = 0 \tag{23}$$

The equivalent control u_{eq} maintaining the system states on the sliding surface is:

$$\begin{aligned} u_{eq} &= -(SB)^{-1}SAx & (24)\\ &= -K_{eq}x & (25) \end{aligned}$$

where SB must be non singular by definition. The next step in the controller synthesis is to operate a coordinate transformation to the state x and obtain a regular form state space realization of (12). Such transformation is necessary to guarantee the existence of $(SB)^{-1}$ in (24). Since $rank(B) = 1$, there exists an orthogonal matrix $T_r \in \mathbb{R}^{4\times 4}$ such that:

$$T_r B = \begin{bmatrix} 0 \\ \tilde{B} \end{bmatrix} \tag{26}$$

with $\tilde{B} \in \mathbb{R} \neq 0$. Thus, T_r is obtained through QR factorization of B. The transformed state is now defined by $\bar{x} = T_r x$ which partitions the system as:

$$\bar{x} = \begin{bmatrix} x_1 \\ x_2 \end{bmatrix} \tag{27}$$

with $x_1 \in \mathbb{R}^3$ and $x_2 \in \mathbb{R}$. Therefor, the linear system (A, B) is written in the new coordinates system:

$$\begin{cases} \dot{x}_1 &= A_{11}x_1 &+A_{12}x_2 \\ \dot{x}_2 &= A_{21}x_1 &+A_{22}x_2 &+\tilde{B}u \end{cases} \tag{28}$$

with

$$T_r A T_r^T = \begin{bmatrix} A_{11} & A_{12} \\ A_{21} & A_{22} \end{bmatrix} \tag{29}$$

The switching function S in the $\bar{x}$ coordinate system written:

$$S T_r^T = [S_1 \;\; S_2] \tag{30}$$

where $S_1 \in \mathbb{R}^{1\times 3}$ and $S_2 \in \mathbb{R}$. Considering (26) and (30), it comes $SB = S_2\tilde{B}$ with $S_2 \neq 0$ ensuring the existence of $(SB)^{-1}$. Assuming the system reaches the sliding motion in (28) we obtain:

$$Sx = S_1x_1 + S_2x_2 = 0 \tag{31}$$

$$x_2 = -Mx_1 \tag{32}$$

where $M = S_2^{-1}S_1$. Equation (28) becomes:

$$\dot{x}_1 = (A_{11} - A_{12}M)\, x_1 \tag{33}$$

From (30), the switching function S is defined as:

$$S = S_2[M \;\; 1]T_r \tag{34}$$

For the sake of simplicity, S_2 is chosen as $S_2 = \tilde{B}^{-1}$ such that $SB = 1$. Finally, M is determined properly by linear quadratic minimization from (33). We now define a positive definite matrix $Q \in \mathbb{R}^{4\times 4}$ and a functional J to minimize:

$$J = \frac{1}{2}\int_{t_s}^{+\infty} x^T Q x \; dt \tag{35}$$

with t_s describing the time for the closed loop to converge to the sliding manifold. Q is then transformed and partitioned in the new coordinate system:

$$T_r Q T_r^T = \begin{bmatrix} Q_{11} & Q_{12} \\ Q_{12}^T & Q_{22} \end{bmatrix} \tag{36}$$

Hence, we choose a suitable virtual control $v = x_2 + Q_{22}^{-1}Q_{12}^T x_1$ and the function J can be written:

$$J = \frac{1}{2}\int_{t_s}^{+\infty} x_1^T \hat{Q} x_1 + v^T Q_{22} v \; dt \tag{37}$$

The virtual control v is finally substituted into $\dot{x}_1$ expression from (28) and it comes

$$\dot{x}_1 = \hat{A}x_1 + A_{12}v \tag{38}$$

with $\hat{Q} = Q_{11} - Q_{12}Q_{22}^{-1}Q_{12}^T$, $\hat{A} = A_{11} - A_{12}Q_{22}^{-1}Q_{12}^T$, and M being the solution to the LQ problem $(\hat{A}, A_{12}, \hat{Q}, Q_{22})$. Once the sliding manifold is defined, the nonlinear control part u_{nl} defined by:

$$u_{nl} = -\rho(SB)^{-1}\frac{\sigma}{|\sigma| + \epsilon} \tag{39}$$

$$= -K_\sigma \frac{\sigma}{|\sigma| + \epsilon} \tag{40}$$

where $\rho \in \mathbb{R}^+$. As for the passivity-based control, the real sliding variable is defined by $\sigma = S\hat{x}$ with $\hat{x}$ the state estimation from (18).

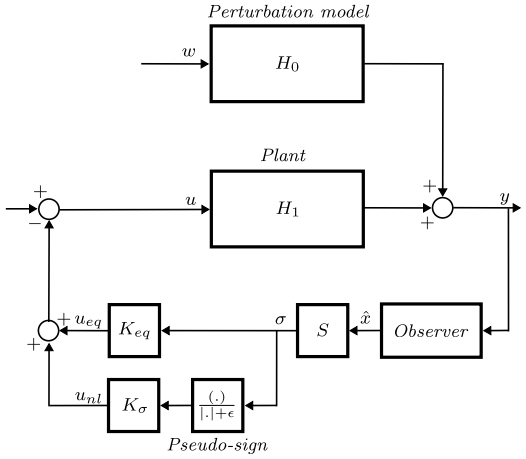

Figure 12: Sliding mode control diagram.

4. Experimental results

The following section will present the experimental results obtained with the four developed controllers on the nominal and uncertain systems A and B.

4.1. Control parameters

First, the Kalman observer of the initial system states x is computed considering the following parameters: $V_d = 1.10^4 \times I_4$ and $V_n = 1$ since the measurement noise is minimum. Hence, the observer gain matrix L^T is solution of the LQR problem (A^T, C^T, V_d, V_n). The same tuning of the observer is used for the α-controller, LQG controller, passivity-based controller and SMC.

Considering the α-controller, the cutt-off frequency parameter ω_{int} affecting the controller $K_\alpha(s)$ and the pseudo-integrator is set at $\omega_{int} = 2\pi$ rad.s^{-1}. In addition, a digital high-pass Chebyshev of order 10 filters the measure y to avoid any remaining continuous component in the control signal. Then, the parameters k_α and α are obtained numerically to minimize the H-infinity norm of the closed-loop system such that $\alpha = 132.5$rad.s^{-1}, $k_{\alpha,A} = 290$, and $k_{\alpha,B} = 522$.

For the LQG controller, the matrix coefficients are $Q = I_4$ and $R = 1.10^{-4}$ and correspond to the best performance achievable without parasitic spill-over phenomenon in the system response.

Considering the passivity-based controller, ϵ is set to 0.1 to avoid a steep function $h(\sigma)$ since no further gain has been observed with strict sign function. The gain k_p is then set to 1.

Finally for SMC, the weighting matrix Q is also set to I_4 and $\epsilon = 10^{-6}$ which is negligible. The parameter defining the switch amplitude ρ is set to 1. As mentioned earlier for the linear quadratic regulator, this amplitude corresponds to the best reachable performance. Therefore, no performance gain is further achieved with a switching amplitude superior to this value. Since the product SB is designed such that $SB = 1$, the gain K_σ equals the value of ρ.

Meanwhile, the SMC equivalent control u_{eq} is set to 0 to assess only the performance and robustness provided by the nonlinear switching control signal.

4.2. Nominal performance

As mentioned in the Subsection 2.1, the proposed controllers are applied first to the nominal systems A and B properly identified. For the perturbation signal, the same band-limited white noise of RMS value 2.21V and sampling frequency of 10kHz is applied to the shaker amplifier like the identification process of H_0. Figure 13 presents the frequency response function $H_{cl}(f)$ of the closed-loop system between the perturbation w and the acceleration measurement y at the end of the beam for system A. One can notice immediately that the LQG controller, the passivity-based controller, and the SMC manage to reduce the system response for some unmodeled dynamics *i.e.* the second bending mode of the cantilever beam. Figure 13b shows accordingly to the previous observation a zoom on the same FRF for bandwidths around the first and second modes. The same results with the nominal system B are displayed in Figure 14.

Considering the nominal systems, all controllers present the same level of attenuation for modeled dynamics (1^{st} bending mode), between -7dB and -8dB compared to the passive TMD. Nevertheless, when it comes to unmodeled dynamics, the α-controller does not affect at all the 2^{nd} mode. On the other hand,

the three other controllers mitigate also the second mode which corresponds to unmodeled dynamics of the system. This is mainly due to the observer since the phase error between the measured transfer function $H_1(f)$ and its simplified model (see Figures 5a and 5b) is reduced at these frequencies, in addition with an observer gain sufficiently high to impact the vibration level.

Nevertheless, SMC displays a superior performance on the second mode compared to the other controllers with system A: up to -25dB. For the nominal system B however, the beam is shortened and its rigidity and modal mass are increased accordingly. Consequently, such configuration leads to a saturation phenomenon in the system controllability due to the limited inertial mass supporting the control effort within the HMD.

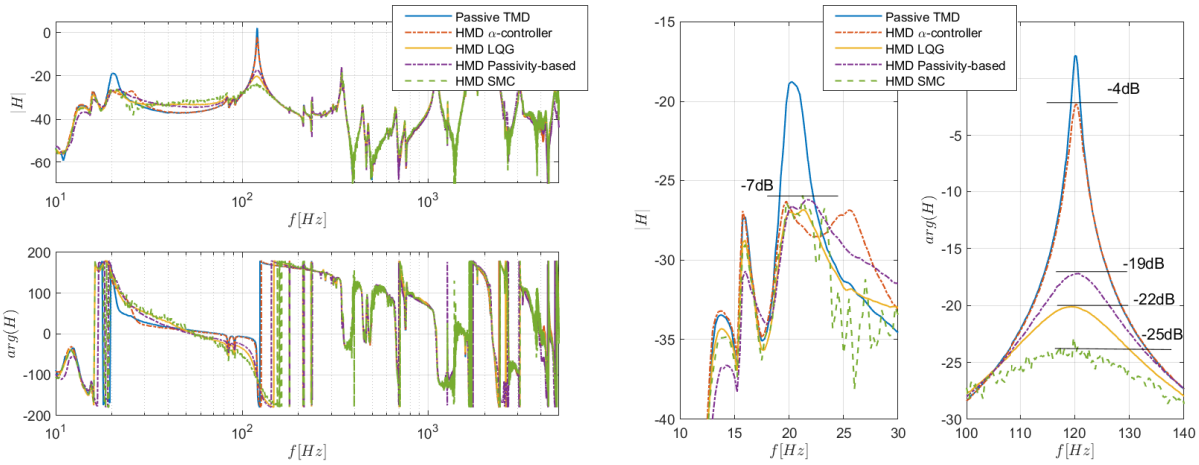

(a) (b)

Figure 13: Transfer functions $H_{cl}(f)$ for nominal system A (a) with zoom on modes 1 and 2 (b).

4.3. Robustness to parametric uncertainties

The following Subsection presents the core result of this manuscript since it highlights the robustness of the SMC method for vibration mitigation on uncertain systems containing modeled and unmodeled dynamics. The same four controllers tuned specifically for nominal systems A or B are now applied to their uncertain versions where the frequencies of the modes are significantly shifted downward (A,-17%) or upward (B,+24%). The Figure 15 displays the FRF $H_{cl}(f)$ for uncertain system A (added mass). It is crucial to emphasize that the observer remains tuned for the nominal system during the transition from the initial to the uncertain one, allowing for an assessment of the robustness of the observer-controller combination.

One can observe that performances for the control of the 1^{st} beam mode now differ from the nominal case. While the SMC maintains a reasonable attenuation

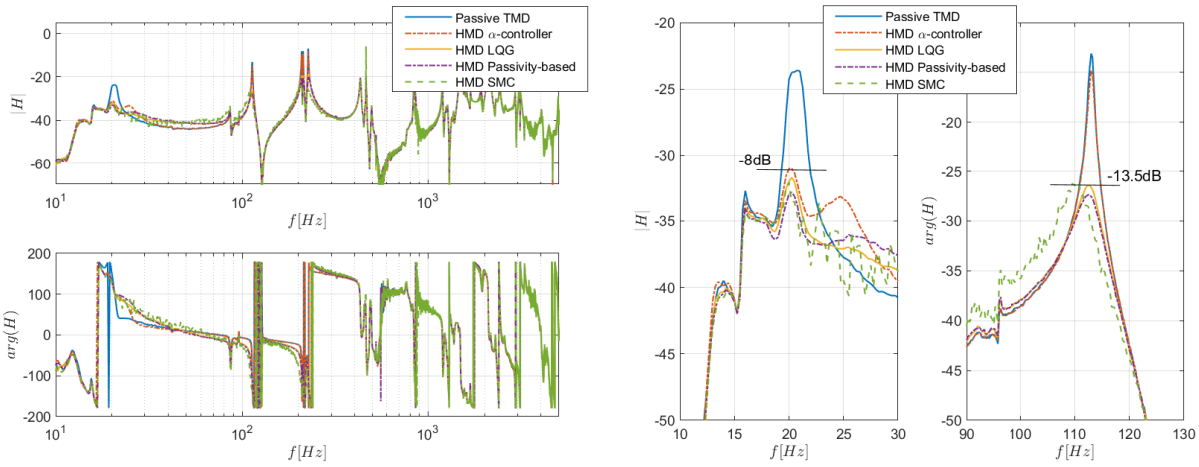

(a) (b)

Figure 14: Transfer functions $H_{cl}(f)$ for nominal system B (a) with zoom on modes 1 and 2 (b).

of -6.5dB corresponding to a performance loss of 0.5dB compared to the nominal system, the other controllers struggle to keep their initial reduction level. For instance, the α-controller even degrades the passive system behavior on the 1^{st} mode of uncertain system B. Considering the 2^{nd} mode, the same conclusions emitted earlier from the nominal case apply where the SMC continues to show superior performance.

Finally, the Figure 16 presents the closed-loop response FRF $H_{cl}(f)$ for the uncertain system B. These last results confirm the robustness of SMC with modeled and unmodeled dynamics compared to other linear methods. It is worth noting that the control performances on the second mode are noticeably superior in the uncertain system B when compared to the nominal system. This improvement can be attributed to the alteration in the mass ratio between the inertial actuator and the beam. In the case of the uncertain system, where mass removal is involved, the HMD encounters less difficulty in effectively mitigating the beam's vibration.

To summarize all the mentioned observations, The Figures 17a and 17b display the level of attenuation in dB for each controller and every system. Taking the LQG method as a reference, the SMC shows an average performance gain of 22.5% on the uncertain systems for both modeled and unmodeled modes, with a maximum of 43% for the 1^{st} mode on uncertain system A.

Lastly, Figure 17c presents for each controller and mechanical system the RMS value of the control signal. Figure 17d displays a time extract of the control signal for each controller on the nominal system A. It is noticeable that since the SMC uses a switching control signal of amplitude ρ, its RMS value is generally much higher. Hence, performance and especially robustness still come

at the cost of control energy. In addition, it is important to emphasize that chattering and its consequences on the mechanical device and noise disconfort is not regarded here. However, adaptive gain for SMC is a possibility to reduce chattering and unnecessary control effort.

Meanwhile, the outcomes are closely linked to the performance of the Kalman observer concerning the LQG, passivity-based controller, and SMC. However, there is an opportunity to enhance the SMC technique by incorporating a robust nonlinear observer, which would undoubtedly yield superior global performance and increased robustness. Finally the Table 2 provides a global overview of the various controllers' assessment based on the experimental results.

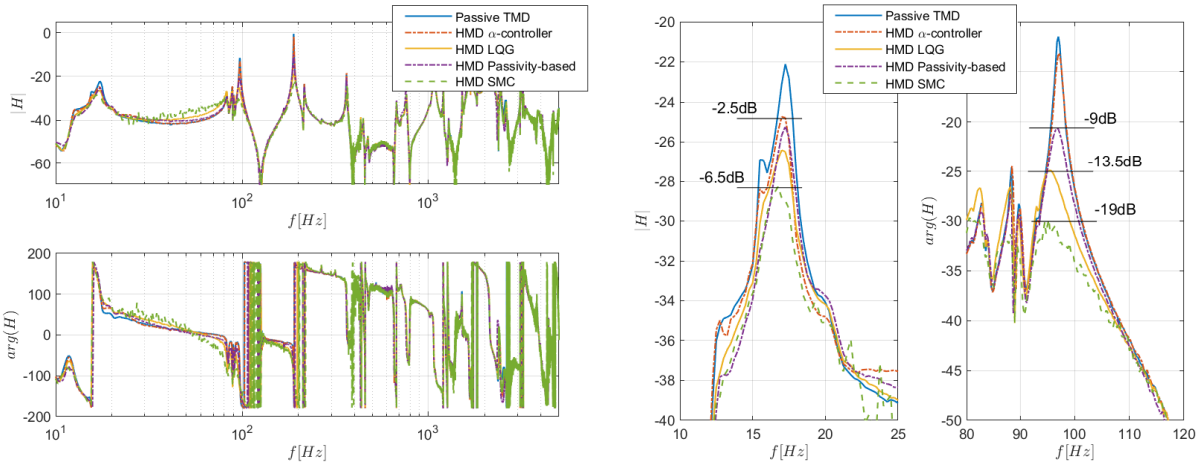

(a) (b)

Figure 15: Transfer functions $H_{cl}(f)$ for uncertain system A (a) with zoom on modes 1 and 2 (b).

5. Conclusion

This paper proposed to experimentally illustrate the advantage of the SMC method for vibration mitigation using Hybrid Mass Dampers over commonly used controllers. The considered dynamic structure was a cantilever beam with the first bending mode located at 21Hz and excited by a shaker. The HMD was a controllable inertial actuator with its internal resonance tuned to the beam first mode. A removable additional mass was used to introduce significant parametric uncertainties. Three different control methods have been compared with SMC: $\alpha-$controller, LQG and passivity-based control, on two nominal and two uncertain systems. If the performances of all controllers were equivalent for well-identified systems, it was not the case when considering unmodeled dynamics and parametric uncertainties causing significant positive and negative shifts in the modal frequencies (-17%/+24% for the first beam mode). Thus, the

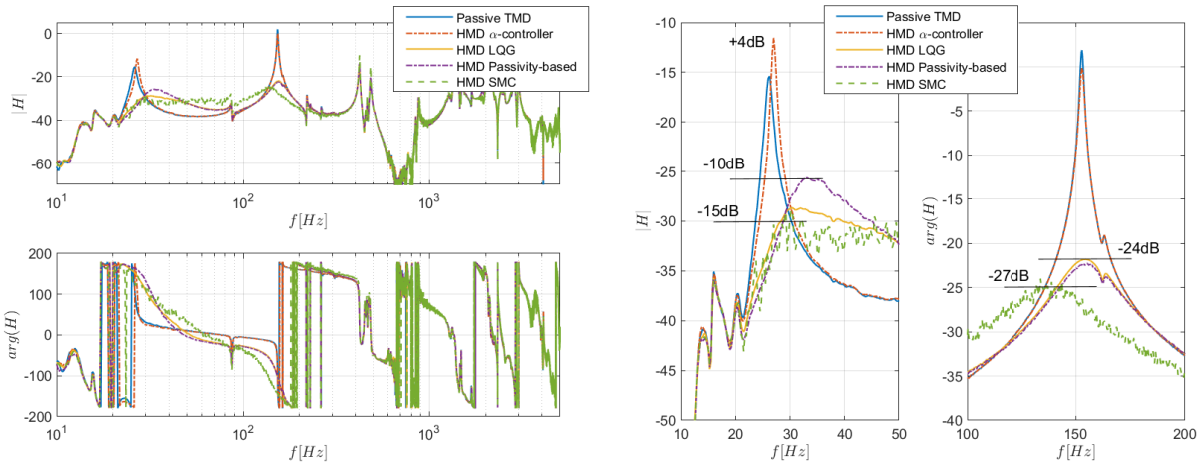

(a) (b)

Figure 16: Transfer functions $H_{cl}(f)$ for uncertain system B (a) with zoom on modes 1 and 2 (b).

experimental results, especially when controlling uncertain systems, highlighted clearly the robustness and performance gain of SMC for vibration mitigation. It is of high importance to recall that such characteristics are highly desirable for active vibration control devices located on transportation systems since their mass and inertia distribution can drastically vary during the one same operating phase. However, it must be mentioned that the highlighted benefits of SMC come at the cost of control energy. Future work will be realized on robust and adaptive observers to further enhance the performance of SMC applied to HMDs while reducing energy consumption and chattering with adaptive methods.

References

[1] J. Sun, M. Jolly, , M. t. Norris, Passive, adaptive and active tuned vibration absorbers—a survey (1995).

[2] A. Preumont, Vibration control of active structures: an introduction, Vol. 246, Springer, 2018.

[3] D. J. Hartog, Mechanical vibrations, McGraw-Hill Book Company, 1956.

[4] T. Asami, O. Nishihara, A. M. Baz, Analytical solutions to h-infinity and h2 optimization of dynamic vibration absorbers attached to damped linear systems, J. Vib. Acoust. 124 (2) (2002) 284–295.

[5] G. Kerschen, M. Peeters, J.-C. Golinval, C. Stéphan, Nonlinear modal analysis of a full-scale aircraft, Journal of Aircraft 50 (5) (2013) 1409–1419.

Control method	Performance	Robustness	Energy cost index (based on Figure 17c)	Implementation
$\alpha-$controller	Localized only on the TMD resonance frequency	Very sensitive to parametric uncertainties	0.01 to 0.05	No observer needed, only velocity or acceleration feedback
LQG control	Superior to $\alpha-$control	Ability to control unmodeled modes while the observer phase is close enough to the real system	0.1	Need of an observer
Passivity-based control	Superior to $\alpha-$control, slightly inferior to LQG	same ability to control unmodeled modes	0.1	Need of an observer
Sliding mode control	Increased performance due to the switching method	Globally higher robustness with unmodeled dynamics and strong parametric uncertainties	1 (arbitrary here, can be decreased using an adaptive gain, however it is usually quite superior to linear control)	Need of an observer, chattering must be handled properly

Table 2: Experimental assessment of the controllers.

[6] K. K. Wong, J. L. Harris, Seismic damage and fragility analysis of structures with tuned mass dampers based on plastic energy, The Structural Design of Tall and Special Buildings 21 (4) (2012) 296–310.

[7] L. Wang, W. Shi, X. Li, Q. Zhang, Y. Zhou, An adaptive-passive retuning device for a pendulum tuned mass damper considering mass uncertainty and optimum frequency, Structural Control and Health Monitoring 26 (7) (2019) e2377.

[8] O. Gendelman, L. I. Manevitch, A. F. Vakakis, R. M'Closkey, Energy pumping in nonlinear mechanical oscillators: part i—dynamics of the underlying hamiltonian systems, J. Appl. Mech. 68 (1) (2001) 34–41.

[9] A. F. Vakakis, O. Gendelman, Energy pumping in nonlinear mechanical oscillators: part ii—resonance capture, J. Appl. Mech. 68 (1) (2001) 42–48.

[10] L. Huo, G. Song, H. Li, K. Grigoriadis, Robust control design of active structural vibration suppression using an active mass damper, Smart materials and structures 17 (1) (2007) 015021.

[11] G. Zhao, G. Raze, A. Paknejad, A. Deraemaeker, G. Kerschen, C. Collette, Active tuned inerter-damper for smart structures and its hinf optimisation, Mechanical Systems and Signal Processing 129 (2019) 470–478.

[12] I. Nishimura, T. Kobori, M. Sakamoto, N. Koshika, K. Sasaki, S. Ohrui, Active tuned mass damper, Smart Materials and Structures 1 (4) (1992) 306.

[13] C. Collette, S. Chesne, Robust hybrid mass damper, Journal of sound and vibration 375 (2016) 19–27.

[14] S. Chesne, G. Inquieté, P. Cranga, F. Legrand, B. Petitjean, Innovative hybrid mass damper for dual-loop controller, Mechanical Systems and Signal Processing 115 (2019) 514–523.

[15] Y. Hu, M. Z. Chen, Y. Sun, Comfort-oriented vehicle suspension design with skyhook inerter configuration, Journal of Sound and Vibration 405 (2017) 34–47.

[16] S. Chesné, Hybrid skyhook mass damper, Mechanics & Industry 22 (2021) 49.

[17] V. Utkin, Methods for constructing discontinous planes in multidimensional variable structure systems, Automation and Remote control 31 (1977) 1466–1470.

[18] K. David Young, Ü. Özgüner, Frequency shaping compensator design for sliding mode, International Journal of Control 57 (5) (1993) 1005–1019.

[19] L. Zuo, J.-J. E. Slotine, Robust vibration isolation via frequency-shaped sliding control and modal decomposition, Journal of Sound and Vibration 285 (4-5) (2005) 1123–1149.

[20] R. Adhikari, H. Yamaguchi, Sliding mode control of buildings with atmd, Earthquake engineering & structural dynamics 26 (4) (1997) 409–422.

[21] J. Rodriguez, M. Collet, S. Chesné, Active vibration control on a smart composite structure using modal-shaped sliding mode control, Journal of Vibration and Acoustics 144 (2) (2022) 021013.

[22] A. Agrawal, J. Yang, J. Wu, Non-linear control strategies for duffing systems, International Journal of Non-Linear Mechanics 33 (5) (1998) 829–841.

[23] M. Soleymani, A. H. Abolmasoumi, H. Bahrami, A. Khalatbari-S, E. Khoshbin, S. Sayahi, Modified sliding mode control of a seismic active mass damper system considering model uncertainties and input time delay, Journal of Vibration and Control 24 (6) (2018) 1051–1064.

[24] A. Concha, S. Thenozhi, R. J. Betancourt, S. K. Gadi, A tuning algorithm for a sliding mode controller of buildings with atmd, Mechanical Systems and Signal Processing 154 (2021) 107539.

[25] J. Ackermann, V. Utkin, Sliding mode control design based on ackermann's formula, IEEE transactions on automatic control 43 (2) (1998) 234–237.

[26] L. Li, G. Song, J. Ou, Adaptive fuzzy sliding mode based active vibration control of a smart beam with mass uncertainty, Structural control and health monitoring 18 (1) (2011) 40–52.

[27] Y. Hu, M. Z. Chen, C. Li, Active structural control for load mitigation of wind turbines via adaptive sliding-mode approach, Journal of the Franklin Institute 354 (11) (2017) 4311–4330.

[28] A. Laub, M. Heath, C. Paige, R. Ward, Computation of system balancing transformations and other applications of simultaneous diagonalization algorithms, IEEE Transactions on Automatic Control 32 (2) (1987) 115–122.

[29] H. K. Khalil, Nonlinear control, Vol. 406, Pearson New York, 2015.

[30] Y. Shtessel, C. Edwards, L. Fridman, A. Levant, et al., Sliding mode control and observation, Vol. 10, Springer, 2014.

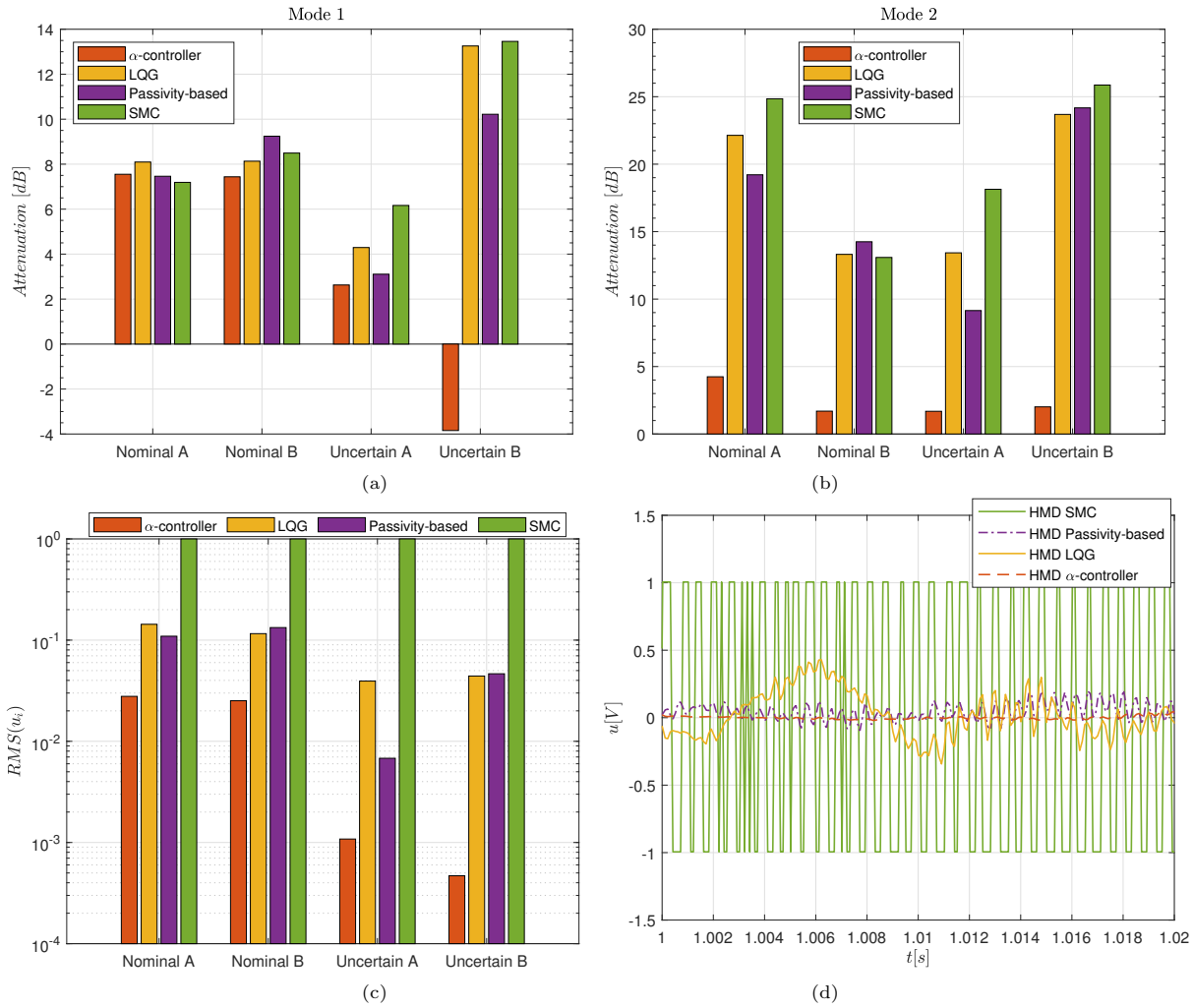

Figure 17: For each controller: attenuation levels for (a) the first beam mode and (b) the second beam mode, (c) RMS value of the control signal u, (d) control signal extract on nominal system A.